Supplementary Information For

Baseline Temperature Variability Shaping Geographical Distribution of Future Hot Extremes under Anthropogenic Warming

Zhili Tang[1], Shenghui Zhou[2], Xiaohui Ma[1,2,*], Lixin Wu[1,2,*], Wenju Cai[1,2,3,4], Zhao Jing[1,2], Zhaohui Chen[1,2], Bolan Gan[1,2]

1. Frontiers Science Center for Deep Ocean Multispheres and Earth System and Key Laboratory of Physical Oceanography, Ocean University of China, Qingdao, China.
2. Laoshan Laboratory, Qingdao, China.
3. State Key Laboratory of Loess and Quaternary Geology, Institute of Earth Environment, Chinese Academy of Sciences, Xi'an, China.
4. State Key Laboratory of Marine Environmental Science & College of Ocean and Earth Sciences, Xiamen University, Xiamen, China

[*]Corresponding author: Xiaohui Ma (maxiaohui@ouc.edu.cn) and Lixin Wu (lxwu@ouc.edu.cn)

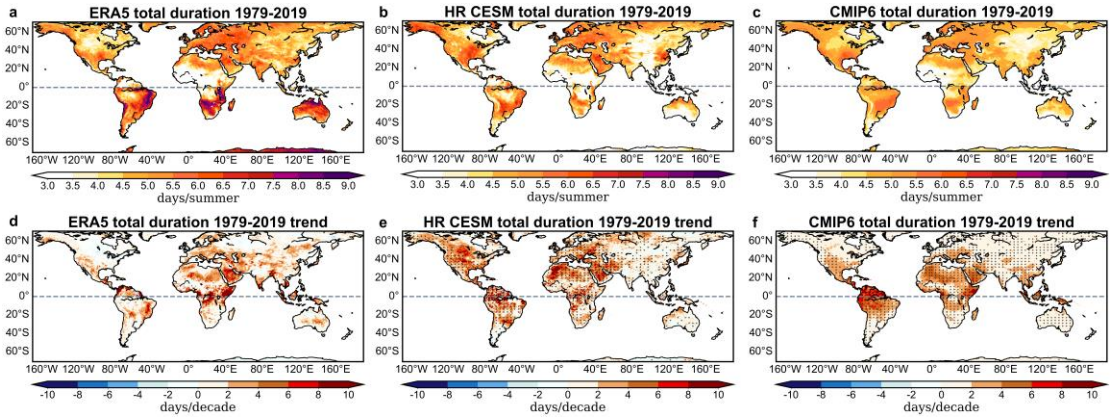

Figure S1 | Observed and simulated hot extremes. Summer season (JJA in the Northern Hemisphere and DJF in the Southern Hemisphere) averages of total duration (days/summer) for hot extreme events in ERA5 (the fifth generation European Center for Medium-Range Weather Forecast atmospheric reanalysis, **a**), HR-CESM (high-resolution Community Earth System Model, **b**) and 10 CMIP6 (Coupled Model Intercomparison Project Phase 6, **c**) simulations during the period 1979-2019. (**d-f**) same as (**a-c**) but for the corresponding trends in hot extreme duration (days/decade) over the same period. Regions where HR-CESM and CMIP6 show a consistent trend with ERA5 are shaded by grey dots in (**e**) and (**f**).

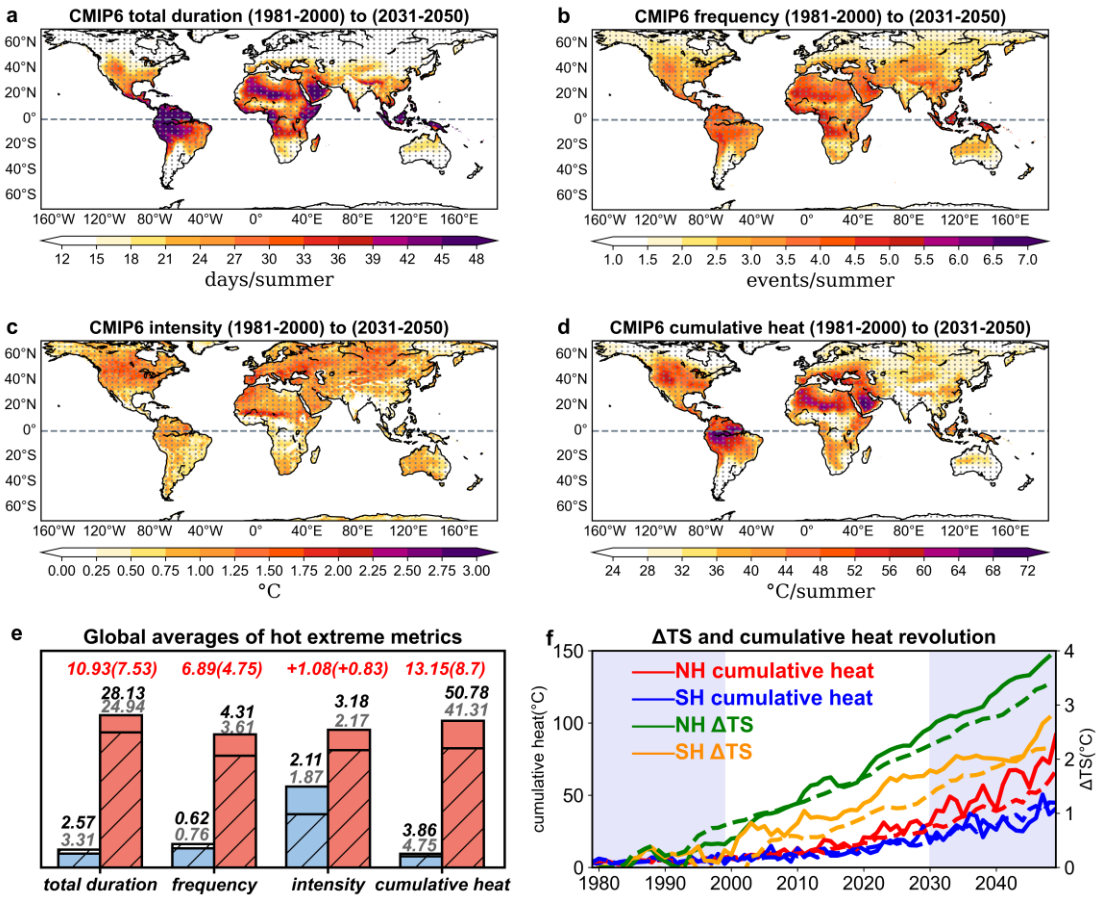

Figure S2 | Responses of hot extremes to anthropogenic warming in CMIP6 (Coupled Model Intercomparison Project Phase 6). Differences in summer season (JJA in the Northern Hemisphere and DJF in the Southern Hemisphere) averages of total duration (days/summer, **a**), frequency (events/summer, **b**), intensity (°C, **c**), and cumulative heat (°C/summer, **d**) for hot extreme events between historical (1981-2000) and future simulations (2031-2050). Differences above the 95% confidence level based on a two-sided Student's test are shaded by gray dots. (**e**) Global averages (70°S-70°N) of hot extreme metrics in historical (blue bars) and future simulations (red bars), with corresponding values labeled above the bars (grey numbers represent CMIP6 results and black numbers represent HR-CESM results). The red numbers at the top indicate the fold increase between future and historical values (CMIP6 results are in parentheses). Hatched bars represent CMIP6 results and solid bars represent HR-CESM results over the same period. (**f**) Time series of cumulative heat averaged for the Northern Hemisphere (15°N-70°N, red line), Southern Hemisphere (15°S-70°S, blue line), along with summer surface temperature changes relative to 1979-1984 (5-year moving average) for the Northern Hemisphere (JJA, 15°N-70°N, green line) and Southern Hemisphere (DJF, 15°S-70°S, orange line). Dashed lines represent CMIP6 results and solid lines represent HR-CESM results. Shaded regions in (**f**) outline the historical and future periods analyzed.

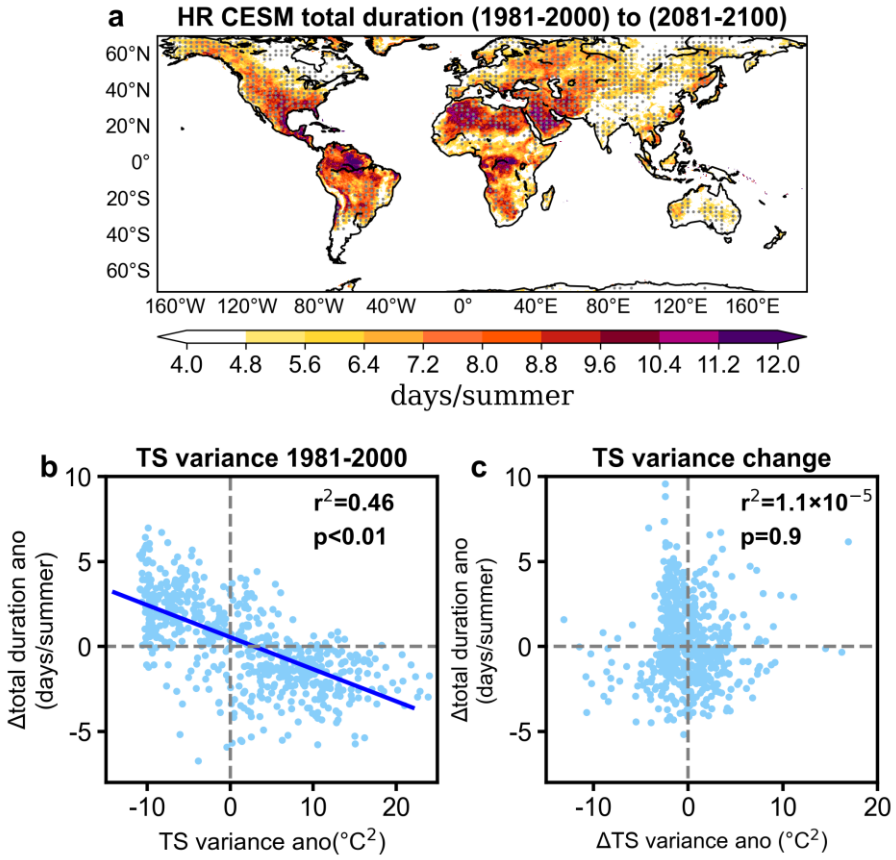

Figure S3 | Sensitivity test of the role of temperature variance in driving the spatial heterogeneity of future hot extremes using a varying threshold. (**a**) Differences in summer season averages of total duration (days/summer) for hot extreme events between historical (1981-2000) and future simulations (2081-2100) in the HR-CESM (high-resolution Community Earth System Model). Hot extreme changes are evaluated using the varying threshold ($T90_{hist}$ and $T90_{future}$, respectively, see Methods for details). Differences above the 95% confidence level based on a two-sided Student's test are shaded by gray dots. (**b**) Scatter plot between anomalous hot extreme total duration changes (future minus historical) and anomalous historical temperature variance (historical) in the regions with negative correlations (covering 71% of the global area). (**c**) Scatter plot between anomalous hot extreme total duration changes (future minus historical) and anomalous temperature variance changes (future minus historical). The anomalous values plotted in (**b**) and (**c**) are computed as the absolute values minus the global mean.

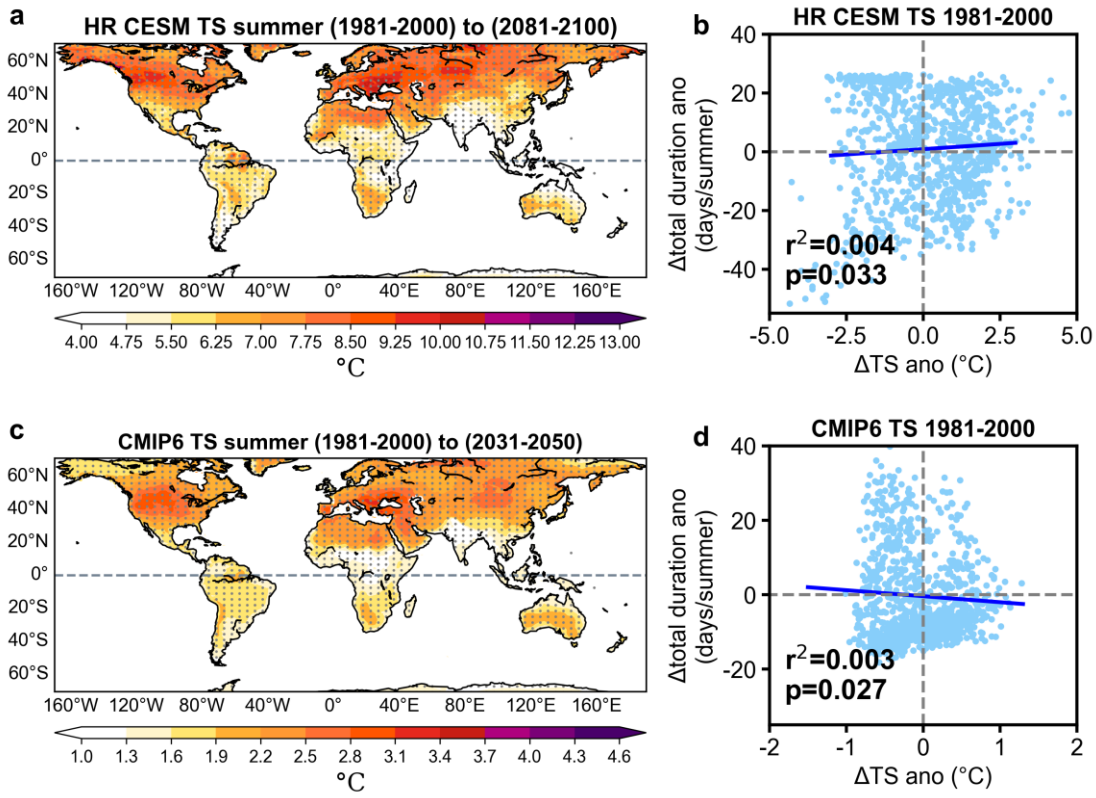

Figure S4 | Role of mean temperature change in driving the spatial heterogeneity of future hot extremes. (**a**) Differences in summer season mean temperature between future (2081-2100) and historical simulations (1981-2000) in HR-CESM (high-resolution Community Earth System Model). (**b**) Scatter plot between anomalous hot extreme total duration changes (future minus historical) and anomalous mean temperature changes (future minus historical) globally (70°N to 70°S). (**c**) and (**d**), same as (**a**) and (**b**), but for future (2031-2050) and historical simulations (1981-2000) in CMIP6 (Coupled Model Intercomparison Project Phase 6). Differences above the 95% confidence level based on a two-sided Student's test are shaded by gray dots in (**a**) and (**c**). The anomalous values plotted in (**b**) and (**d**) are computed as the absolute values minus the global mean.

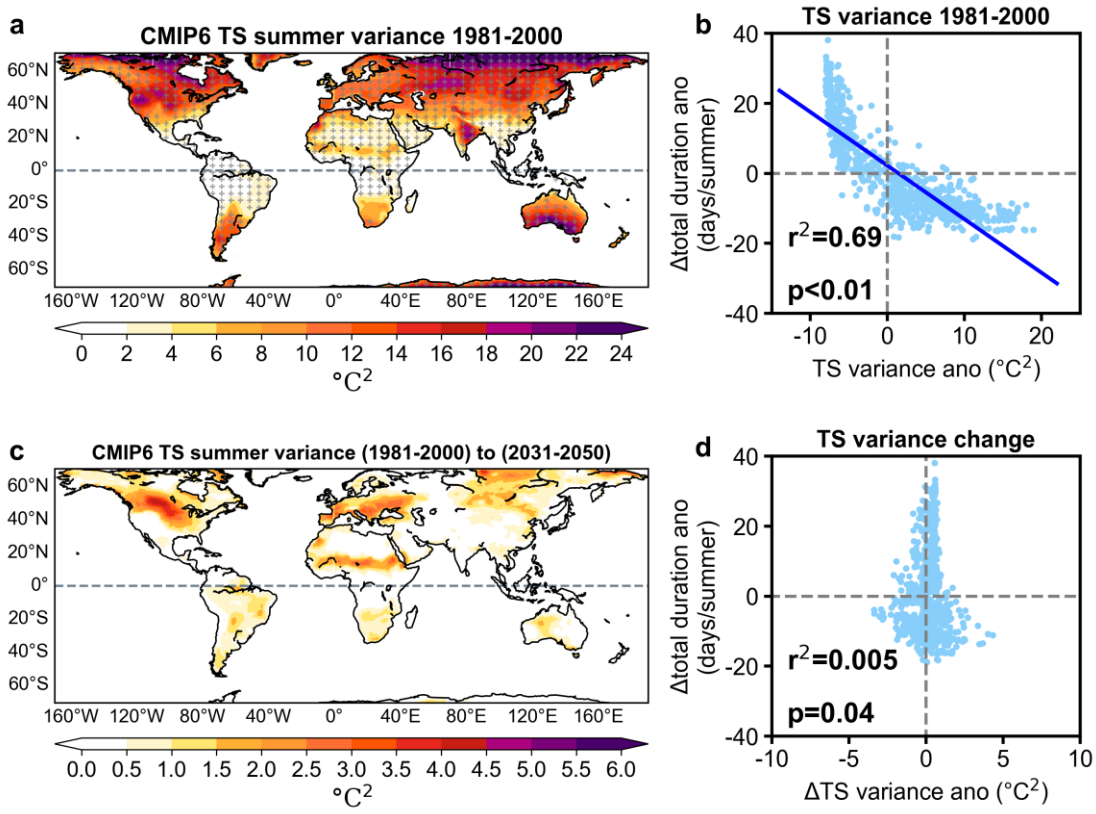

Figure S5 | Role of temperature variance in driving the spatial heterogeneity of future hot extremes in CMIP6 (Coupled Model Intercomparison Project Phase 6). Summer season averaged temperature variance in historical simulations (1981-2000, **a**) and the difference of that between future (2031-2050) and historical simulations (1981-2000) in CMIP6 (**c**). Regions with a negative correlation between hot extreme change and historical temperature variance are shaded by plus markers in (**a**). (**b**) Scatter plot between anomalous hot extreme total duration changes (future minus historical) and anomalous historical temperature variance (historical) in the regions with negative correlations (covering 93% of the global area). (**d**) Scatter plot between anomalous hot extreme duration changes (future minus historical) and anomalous temperature variance changes (future minus historical). The anomalous values plotted in (**b**) and (**d**) are computed as the absolute values minus the global mean.

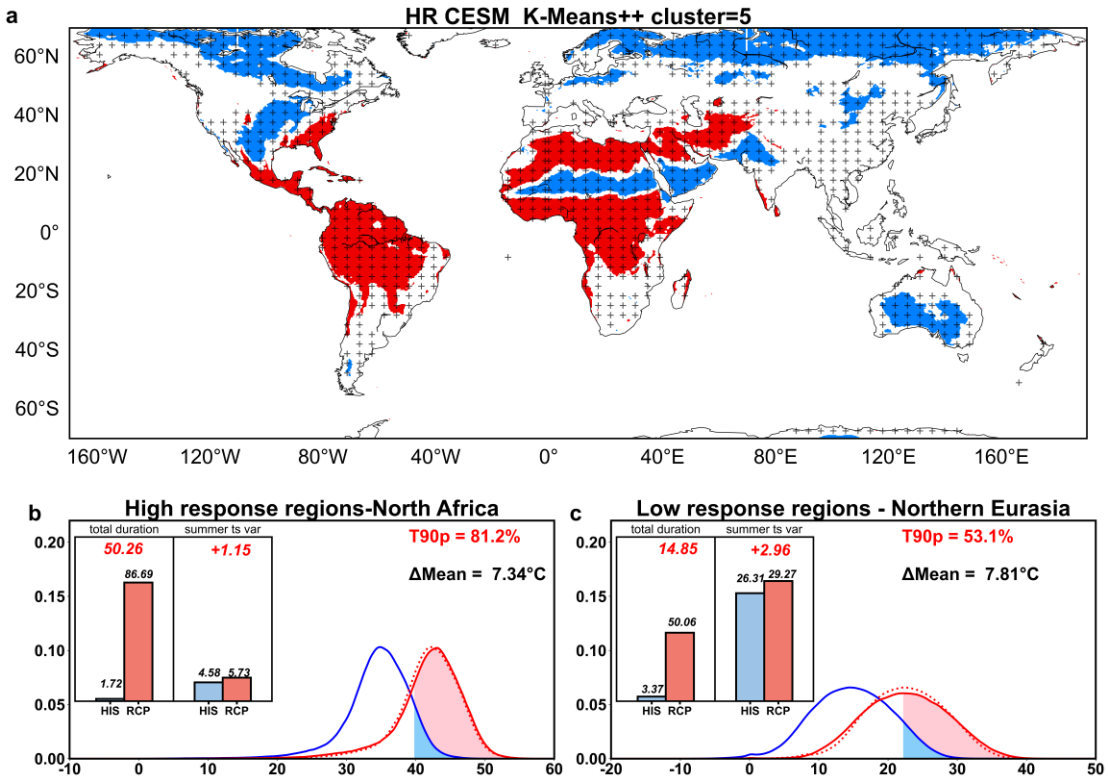

Figure S6 | High-response and low-response regions identified by K-means clustering. (**a**) High-response (red) and low-response (blue) regions for hot extreme projection in HR-CESM (high-resolution Community Earth System Model) are identified using K-means clustering (Methods). Regions with a negative correlation between hot extreme change and historical temperature variance are shaded by plus markers. Temperature probability distribution functions (PDFs) for North Africa (**b**) and Northern Eurasia (**c**) in historical (blue solid line) and future (red solid line) simulations in HR-CESM. The red dashed line represents the shifted PDF corresponding to the mean temperature change. Bar plots show region-averaged total duration and temperature variance for historical (blue) and future (red) periods, with corresponding values and fold increases labeled above the bars.

Table. S1 Models selected from the Coupled Model Intercomparison Project Phase 6 (CMIP6), including five high-resolution (HR) simulations from the High-Resolution Model Intercomparison Project (HighResMIP) and five pairing low-resolution (LR) simulations. Each model includes a 100-year historical and future (under RCP8.5 scenario) simulation from 1950-2050.

Model	Atmospheric Resolution	Oceanic Resolution	Period
CNRM-CM6-1	LR: T127 (~100km)	LR: 1˚	1950-2050
	HR: T359(~35km)	HR: 0.25˚	
EC-Earth3P	LR: T255 (~80km)	LR: 1˚	1950-2050
	HR: T511 (~40km)	HR: 0.25˚	
FGOALS-f3	LR: 100km	LR: 0.25˚	1950-2050
	HR: 25km	HR: 0.1˚	
HadGEM3-GC31	LR: 250km	LR: 1˚	1950-2050
	HR: 60km	HR: 0.25˚	
MPI-ESM1-2	LR: T127 (~100km)	LR: 0.4˚	1950-2050
	HR: T255 (~25km)	HR: 0.4˚	